Plane-strain bulge test for thin films

Y. Xiang
Division of Engineering and Applied Sciences, Harvard University, Cambridge, Massachusetts 02138-2901

X. Chen
Department of Civil Engineering and Engineering Mechanics, Columbia University, New York, New York 10027-6699

J.J. Vlassak[a)]
Division of Engineering and Applied Sciences, Harvard University, Cambridge, Massachusetts 02138-2901

(Received 21 January 2005; accepted 19 April 2005)

The plane-strain bulge test is a powerful new technique for measuring the mechanical properties of thin films. In this technique, the stress–strain curve of a thin film is determined from the pressure-deflection behavior of a long rectangular membrane made of the film of interest. For a thin membrane in a state of plane strain, film stress and stain are distributed uniformly across the membrane width, and simple analytical formulae for stress and strain can be established. This makes the plane-strain bulge test ideal for studying the mechanical behavior of thin films in both the elastic and plastic regimes. Finite element analysis confirms that the plane-strain condition holds for rectangular membranes with aspect ratios greater than 4 and that the simple formulae are highly accurate for materials with strain-hardening exponents ranging from 0 to 0.5. The residual stress in the film mainly affects the elastic deflection of the membrane and changes the initial point of yield in the plane-strain stress–strain curve, but has little or no effect on further plastic deformation. The effect of the residual stress can be eliminated by converting the plane-strain curve into the equivalent uniaxial stress–strain relationship using effective stress and strain. As an example, the technique was applied to an electroplated Cu film. Si micromachining was used to fabricate freestanding Cu membranes. Typical experimental results for the Cu film are presented. The data analysis is in good agreement with finite element calculations.

I. INTRODUCTION

Thin films have many important applications in modern industries.[1,2] For example, thin films with thicknesses well below 1 μm are widely used as functional and structural elements in ultra-large-scale integrated circuits and microelectromechanical systems, as well as in newly emerging nano-devices and biomedical devices. Thicker films are often used as wear-resistant coatings on cutting tools, protective coatings in data storage devices, and thermal-barrier coatings on turbine blades. To take full advantage of these materials and to further improve their reliability, the mechanical behavior of thin films must be well understood. It is well known that many materials behave very differently in thin film form than they do in the bulk.[3] For example, thin metal films are often found to support much higher stresses than the same material in bulk form, and their yield stress scales inversely with film thickness if the film surface is passivated.[4,5] Besides the size effects associated with film thickness, mechanical properties also depend strongly on film microstructure and fabrication process.[6] Consequently, the mechanical properties of thin films need to be characterized carefully to obtain accurate values.

The traditional mechanical testing methods used for bulk materials cannot be applied directly to the study of thin films because of the small dimensions of these materials. Several specialized techniques have been developed to characterize the mechanical behavior of thin films during past decades. Among them, the substrate curvature[1] and nanoindentation[7] techniques are the most widely used and commercialized. These two techniques involve little sample preparation since they directly test thin films deposited on substrates. The information that

[a)]Address all correspondence to this author.
e-mail: vlassak@esag.deas.harvard.edu
DOI: 10.1557/JMR.2005.0313

can be acquired from these techniques is, however, limited. For example, nanoindentation is often affected by the presence of the substrate, and it is not suitable for measuring the work-hardening behavior or the residual stress in the film.[8,9] In the substrate curvature technique, the film strain can only be changed by changing the temperature, thus making it difficult to interpret the results.[10] Among techniques developed to measure the mechanical behavior of freestanding thin films, the microtensile test[11–14] and the bulge test techniques[15] are widely used. These techniques require some sample preparation, but they can be readily applied to measure intrinsic film properties without any substrate effects and to obtain thin film constitutive behavior with relatively large applied strains. The microtensile test is the analog of its bulk counterpart. Due to difficulties associated with sample handling at the micron or submicron scale, microtensile testing often suffers from alignment and gripping problems, although progress has been made by using Si micromachining techniques to fabricate tensile specimens.[11,13] In the bulge test, freestanding thin films are obtained by opening a window in the substrate using micromachining techniques. The freestanding film is deflected by applying a uniform pressure to the film. The mechanical properties of the film are determined from its pressure-deflection behavior. Compared with microtensile testing, the bulge test technique has the unique advantage of precise sample fabrication and minimal sample handling. With some care, freestanding films as thin as 100 mm films can be prepared and tested.

Bulge testing of thin films was first reported by Beams in 1959, as a technique for measuring in-plane mechanical properties of thin films.[16] In the beginning, the technique suffered from a number of problems related to sample processing, handling, and data analysis. The recent rapid development of silicon micromachining technology has made it possible to manufacture bulge test samples with precisely controlled dimensions and has dramatically reduced sample handling.[15,17] These improvements have made accurate bulge testing possible. To explain the experimental data and relate them to the mechanical properties of the tested films, both theoretical and numerical analyses have been conducted to understand the pressure–deflection relation for membranes with various shapes. Hencky was the first to publish an analytical solution for the elastic deflection of a pressurized circular membrane with fixed edges.[18] Vlassak generalized Hencky's solution to include the influence of residual stress on the deflection of a membrane.[19] The problem becomes more complex for noncircular geometries such as square or rectangular membranes. An exact elastic solution for the problem of a pressurized square membrane was given by Levy but is too complex to be practically useful.[20] A number of researchers have developed approximate solutions using energy minimization methods.[15,17,21,22] Vlassak and Nix[15] derived an accurate expression for the elastic load–deflection behavior of square and rectangular membranes following an approach originally developed by Timoshenko.[22] The effect of residual stress on the membrane deflection was also taken into account. These researchers further found that once the aspect ratio of a rectangular membrane exceeds 4, the deflection at the center of the membrane is nearly independent of the aspect ratio and can be approximated with the exact solution for an infinitely long rectangular membrane, which can be readily derived.[15,22]

The accuracy and reliability of the bulge test has been analyzed by a number of researchers. Itozaki showed that failure to include the initial height of the membrane in the analysis leads to an apparent nonlinear elastic behavior of the film.[23] Small et al. analyzed the influence of initial film conditions such as film wrinkling, residual stress, and initial height of the membrane using finite element analysis.[24,25] Vlassak[19] investigated the contribution of the film bending stiffness to the deflection of a membrane. He showed that for typical bulge test geometries, the bending moment is only significant very close to the edge of the membrane and is negligible everywhere else. These analyses, together with new sample preparation techniques based on Si micromachining, have made the bulge test a useful technique to accurately measure the elastic properties of both freestanding films and multilayers across a wide range of materials, including ceramics, metals, polymers, etc.[15,26–28]

Because the bulge test technique measures isothermal stress-strain curves of freestanding films, it is also ideal for studying plasticity in thin films. Mathematical analyses of the bulge test, however, are based on linear elasticity and may not be applied to the plastic regime. In circular, square, or rectangular membranes with small-aspect ratios, the stress and strain in the film are not uniform.[19] As a result, plastic flow does not initiate uniformly in the membrane. Even after the entire membrane has yielded, different parts of the membrane undergo different amounts of plastic deformation, and the resulting stress state in the film can be quite complex. These geometries are thus not suitable for studying the plastic properties of thin films. We will show that deformation of rectangular membranes with aspect ratios greater than 4 results in a state that closely approximates plane strain. For thin films in a state of plane strain, the stress and strain are distributed uniformly across the width of the membrane. This feature makes long rectangular membranes especially useful for studying the plastic behavior of thin films. Indeed, a similar approach has been used to study work hardening in thin sheets, although the test geometry is quite different in this case.[33]

Simple analytical formulae are established to calculate the stress and strain independently from the applied

pressure and the deflection at the center of the membrane.[19] There has been, however, no systematic study of the accuracy of these formulae in the plastic regime. In this study, we first review the equations used to analyze bulge test results. Then, a finite element analysis is carried out to verify the accuracy of these equations in the plastic regime. A sample preparation process based on silicon micromachining technology is used to manufacture long rectangular freestanding Cu membranes. Typical experimental results and data analyses for the Cu thin films are demonstrated and compared with the results from the finite element analysis.

II. ANALYSIS

Consider a pressurized rectangular membrane made of an isotropic elastic-plastic material with a power-law stress–stain relationship. Figure 1(a) shows a perspective view of the membrane before and after pressure is applied; Fig. 1(b) is a plan view of the membrane window framed by a Si substrate. The deflection h at the center of a membrane of dimensions $2a \times 2b$ is a function of the applied pressure, various material parameters, and the membrane geometry

$$h = f(p, \sigma_0, E, \sigma_y, \nu, n, a, b, t) \quad , \tag{1}$$

where p is the applied pressure, σ_0 the in-plane equibiaxial residual stress in the film, E Young's modulus, ν Poisson's ratio, σ_y the yield stress, n the strain-hardening exponent, and t the film thickness. The dimensionless form of the above function is

$$\frac{h}{a} = F\left(\frac{p}{E}, \frac{\sigma_0}{\sigma_y}, \frac{\sigma_y}{E}, \nu, n, \frac{b}{a}, \frac{t}{a}\right) \quad . \tag{2}$$

In the elastic regime, the strain-hardening exponent and the yield stress do not enter the equation and Eq. (2) is reduced to

$$\frac{h}{a} = F_1\left(\frac{p}{E}, \frac{\sigma_0}{E}, \nu, \frac{b}{a}, \frac{t}{a}\right) \quad . \tag{3}$$

For a linear elastic membrane, this relationship is well approximated by the following functional form[15,19,21]

$$p = c_1(b/a)\,\frac{\sigma_0 t}{a^2}\,h + c_2(\nu, b/a)\,\frac{Et}{(1-\nu)a^4}\,h^3 \quad , \tag{4}$$

where c_1 is a constant that depends on the aspect ratio b/a, and c_2 a constant that depends on both Poisson's ratio and the membrane aspect ratio. The above equation is based on the membrane assumption, i.e., the influence of the bending stiffness of a membrane is negligible compared to the contribution of the residual stress. This is so if $(\sigma_0/E)(a^2/t^2)$.[1] It can be shown with a boundary layer analysis that in this case the effect of the bending stiffness is to reduce the deflection of the membrane by an amount less than the film thickness.[19] The sample dimensions in the present study satisfy this membrane assumption. For rectangular membranes with aspect ratios greater than 4, the assumption of plane strain holds and the pressure-deflection relationship is found to be

$$p = 2\,\frac{\sigma_0 t}{a^2}\,h + \frac{4}{3}\,\frac{Et}{(1-\nu^2)a^4}\,h^3 \quad , \tag{5}$$

where $2a$ is the width of the membrane, as shown in Fig. 1(a).

The linear elastic analysis becomes invalid once the film deforms plastically. When subjected to uniform pressure, an infinitely long membrane with negligible bending stiffness takes the shape of a section of a cylinder with a circular cross-section.[19] The stress and strain in the membrane are then uniform across the width of the

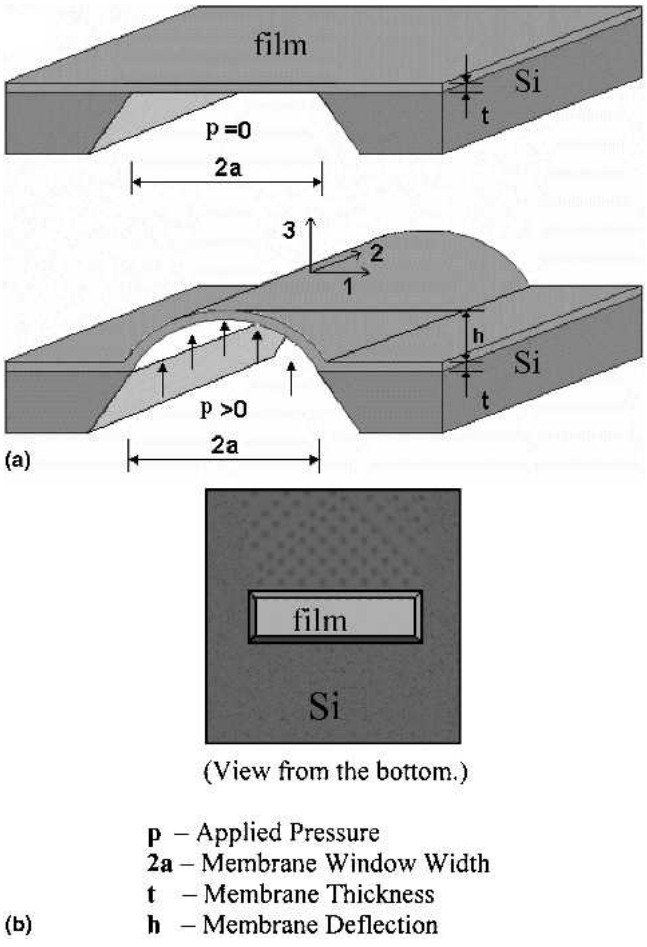

FIG. 1. Schematic illustration of the plane-strain bulge test for a long rectangular membrane: (a) perspective view of the freestanding film before and after the pressure (p) is applied and (b) plan view of a typical sample showing a long rectangular membrane framed by a Si substrate.

membrane independent of whether the film deforms elastically or plastically, and are given by

$$\sigma = \frac{p(a^2 + h^2)}{2ht} \text{ and}$$
$$\epsilon = \epsilon_0 + \frac{a^2 + h^2}{2ah} \arcsin\left(\frac{2ah}{a^2 + h^2}\right) - 1 \quad , \qquad (6)$$

where ϵ_0 is the residual plane strain in the film. When the deflection is much smaller than the membrane width, i.e., $h \ll a$, the above equations reduce to

$$\sigma = \frac{pa^2}{2ht} \text{ and } \epsilon = \epsilon_0 + \frac{2h^2}{3a^2} \quad . \qquad (7)$$

For strains less than 1% and the membrane aspect ratios used in this study, the difference between Eqs. (6) and (7) is negligible. When the deflection h is large compared to a, Eq. (6) should be used.

Because there is no analytical solution for the plastic deflection of rectangular membranes of finite length, the finite element method (FEM) is used to evaluate the accuracy of Eqs. (6) and (7). The parameters governing plastic deformation of the membrane are given in Eq. (2). Since we are interested in the plastic flow behavior of very thin films, the effects of b/a, n, and σ_0/σ_y are examined only for the limit where $t \ll 2a$. Finite element calculations are performed using the commercial code ABAQUS. Plastic deformation is modeled using a large-deformation description combined with J_2 flow theory. The rectangular membrane is represented by 1000 three-dimensional, eight-node, quadratic, thin-shell elements (element S8R5, with 5 degrees of freedom at each node and with reduced integration) that account for finite rotations of the middle surface. The thin film is made of an elastic-plastic material governed by a power-law constitutive equation with a strain-hardening exponent n in uniaxial tension

$$\frac{\sigma}{\sigma_y} = \frac{\epsilon}{\epsilon_y}, \text{ when } \sigma < \sigma_y \quad ,$$
$$\frac{\sigma}{\sigma_y} = \left(\frac{\epsilon}{\epsilon_y}\right)^n, \text{ when } \sigma > \sigma_y \quad . \qquad (8)$$

The edges of the membrane are assumed to be clamped since the substrate suppresses any rotation of the edges.

Using this finite element model, the deflection at the center of a rectangular membrane is calculated as a function of applied pressure, membrane aspect ratio, and work-hardening exponent. The residual stress was fixed at 60% of the yield stress; the elastic modulus was taken to be 1200 times the yield stress; the t/a ratio was 3×10^{-3}. The resulting pressure–deflection relationships are converted into plane-strain stress–strain curves using Eq. (6) and plotted in Fig. 2. These curves are then compared with the plane-strain stress–strain relationship directly calculated from the uniaxial behavior in Eq. (8)

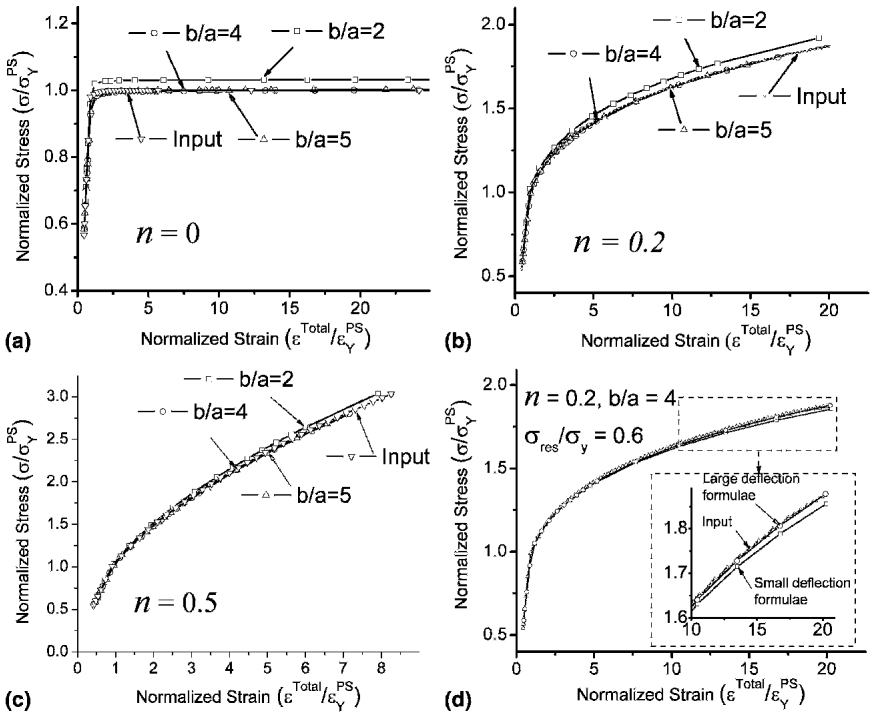

FIG. 2. Plane-strain stress–strain curves obtained from the finite element method for various aspect ratios (b/a = 2, 4, and 5) and for (a) n = 0, (b) n = 0.2, and (c) n = 0.5; (d) plane-strain stress–strain curves calculated using small and large deformation formulae for a membrane with n = 0.2 and b/a = 4.

using finite elements and denoted by "input" in Fig. 2. All stresses in Fig. 2 are normalized by the plane-strain yield stress σ_Y^{PS}, defined as the yield stress for the input plane-strain stress–strain curve calculated using finite elements; the strains are normalized by the corresponding yield strain (ϵ_Y^{PS}). The numerical results for the plane-strain σ–ϵ relationships are presented in Figs. 2(a), 2(b), and 2(c), for $n = 0$, 0.2, 0.5, respectively. For each value of n, stress–strain curves obtained from membranes with three different aspect ratios are compared with the input material behavior. It can be seen that for all strain-hardening exponents considered in this study, the transverse stress and strain predicted from Eq. (6) are highly accurate as long as the membrane aspect ratio is at least 4. Even membranes with $b/a = 2$ show good agreement, especially for larger values of the work-hardening exponent. To illustrate the difference between small and large deformation formulae, Fig 2(d) shows the stress–strain curves calculated using both sets of equations for a membrane with $b/a = 4$. As expected, both curves coincide with the input curve when the applied strain is small. At a strain of 1%, the σ–ϵ relationship calculated using the small deformation formulae [Eq. (7)], is approximately 1.5% lower than the input curve; the curve calculated using the large deformation formulae [Eq. (6)] is indistinguishable from the input curve at both small and large strains. The FEM output data also verify that the longitudinal strain does not change with the applied strain, i.e., the plane-strain condition is well satisfied, and the transverse stress and strain are distributed uniformly across the width of the membrane for membranes with aspect ratios equal to or greater than 4.

The effect of the residual stress on the plane-strain bulge test was also investigated using the finite element method. Figure 3 shows the pressure–deflection curves for films with various levels of residual stress and the corresponding plane-strain stress–strain curves obtained using Eq. (6) for both ideally plastic [Figs. 3(a) and 3(b)] and strain-hardening [Figs. 3(c) and 3(d)] materials. It is found that the residual stress affects mainly the elastic deflection [Figs. 3(a) and 3(c)] and the initial point of yield [Figs. 3(b) and 3(d)] as expected from the yield criterion. If the material obeys the von Mises yield criterion, the stress at first yield varies from the uniaxial yield stress σ_y[9], if the residual stress is equal to the yield stress, to $\sigma_y/\sqrt{1-\nu+\nu^2}$ if the residual stress is zero. Once the film deforms plastically, the effect of the residual stress is quickly wiped out. For ideally plastic materials, the residual stress has no effect on the rest of the stress–strain curve [Fig. 3(b)]; for strain-hardening materials, the effect amounts to a small shift along the strain axis [Fig. 3(d)]. The plane-strain stress–strain curves [Figs. 3(b) and 3(d)] can be converted into equivalent stress-equivalent strain curves [Figs. 4(a) and 4(b)], using the method described in the Appendix. The small discrepancy caused by the biaxial residual stress in the plane-strain stress–strain curves is completely eliminated in the equivalent uniaxial stress–strain curves.

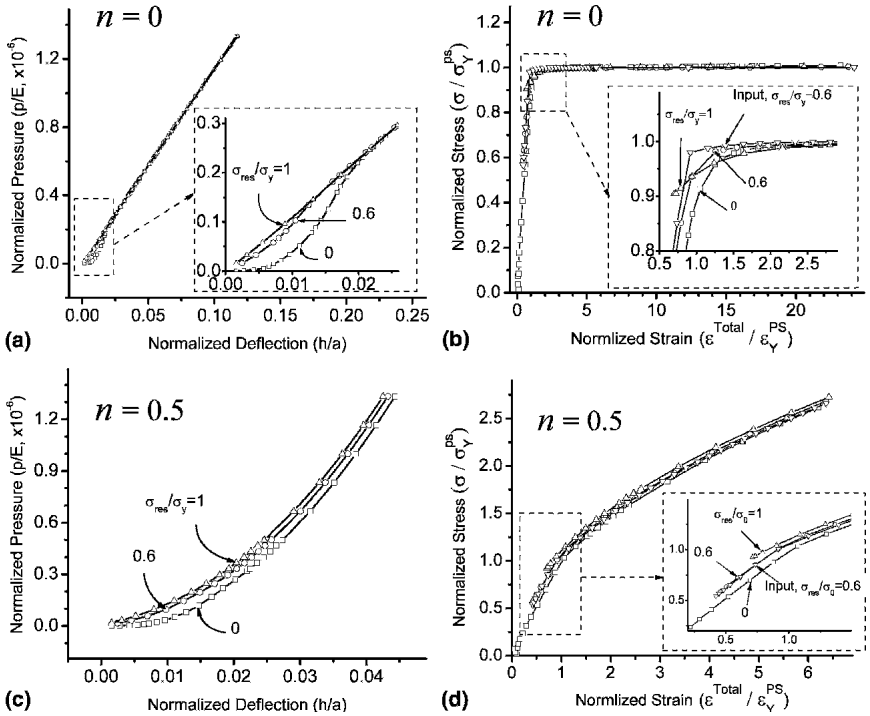

FIG. 3. Pressure–deflection curves and corresponding plane-strain stress–strain curves obtained from the finite element method for an ideally plastic material [(a,b) $n = 0$] and a strain-hardening material [(c,d) $n = 0.5$] with various levels of residual stress ($\sigma_{res}/\sigma_y = 0$, 0.6, and 1).

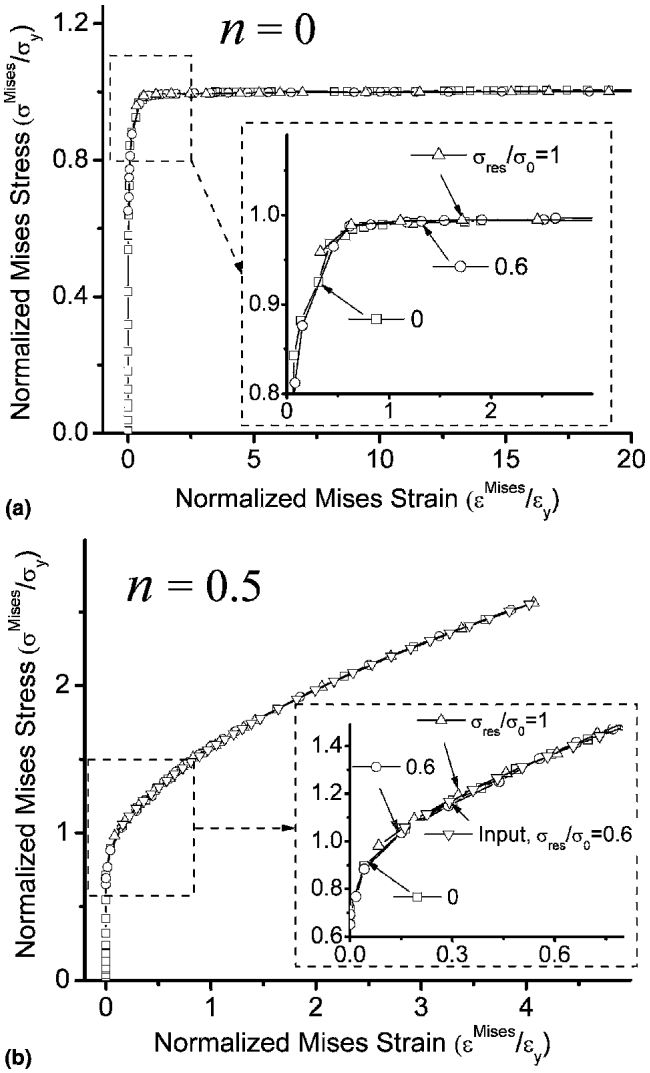

FIG. 4. The von Mises stress-strain curves for the ideally plastic material [(a) $n = 0$, corresponding to Fig. 3(b)] and strain-hardening material [(b) $n = 0.5$, corresponding to Fig. 3(d)] with various levels of residual stress ($\sigma_{res}/\sigma_y = 0$, 0.6, and 1).

III. SAMPLE PREPARATION

In this study, a 2.8-μm electroplated Cu film was tested to illustrate the methodology of the plane-strain bulge test. Freestanding Cu membranes were prepared using standard photolithography and silicon micromachining techniques. As shown in Fig. 5, we start with a (100) Si wafer coated on both sides with low-pressure chemical vapor deposited (LPCVD) Si_3N_4 film. First, a 30-nm TaN adhesive layer and a thin Cu seed layer were sputter deposited onto the Si_3N_4 followed by electrodeposition of the Cu film. The as-deposited film was annealed for 1 h in vacuum at 600 °C to stabilize the microstructure. A detailed microstructural characterization of the film has been published elsewhere.[29] A layer of benzocyclobutene (BCB) was spincoated onto the Cu film to protect it during subsequent processing.

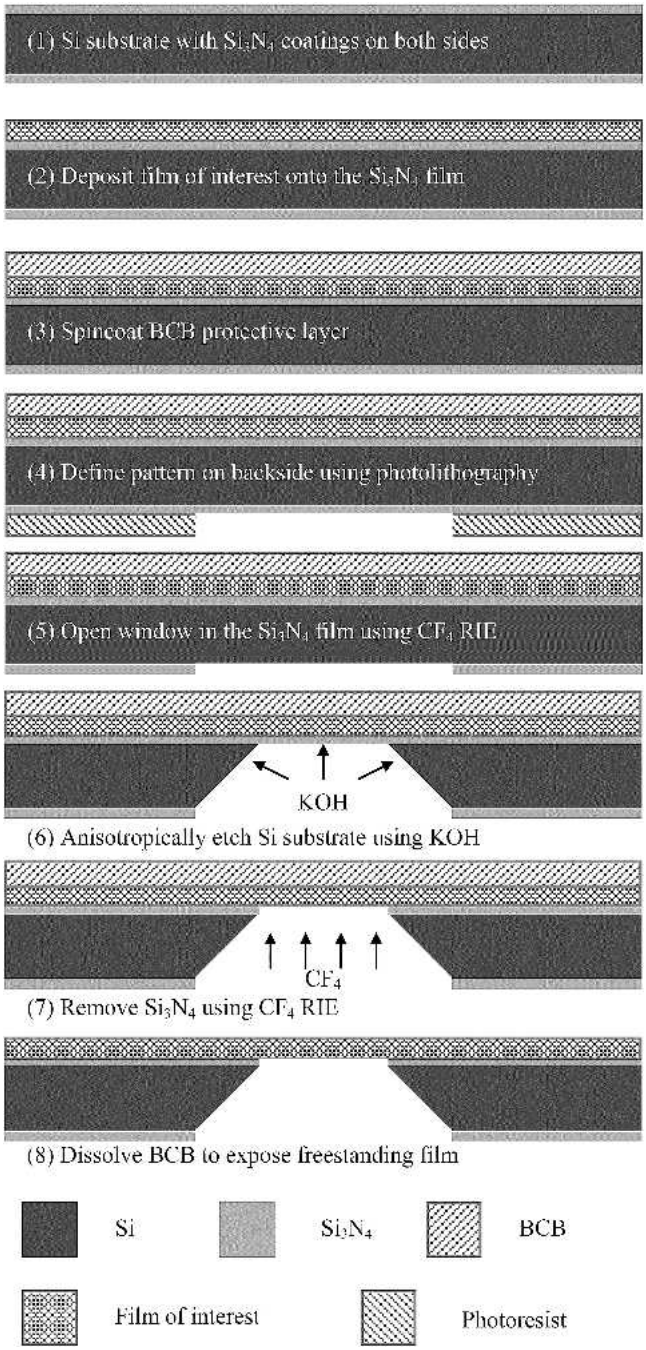

FIG. 5. Schematic illustration of the sample preparation process using standard photolithography and Si micromachining technology.

Photolithography is used to define long rectangular windows (with an aspect ratio of 4:1) in the LPCVD Si_3N_4 coating on the backside of the substrate and with the edges of the rectangles aligned along the ⟨110⟩ directions in the Si substrate. The Si substrate is etched anisotropically [etch selectivity between (100) and (111) crystal plane is approximately 50:1] using a potassium hydroxide (KOH) based wet etch to create freestanding membranes that consist of the Si_3N_4 coating and the Cu film. The size of the membranes is 2.4 × 10 mm^2 (with $2a$ =

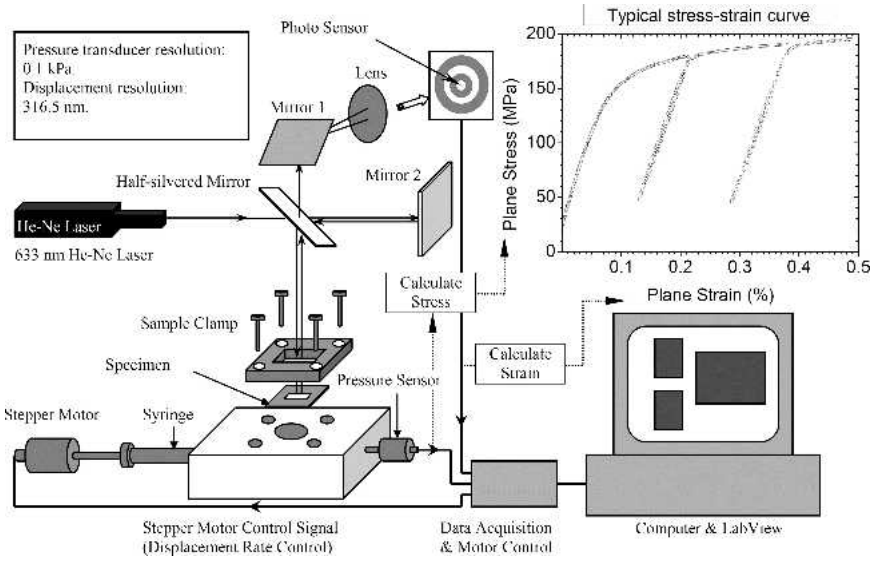

FIG. 6. Schematic illustration of the bulge test apparatus.

2.4 mm in Fig. 1). Finally, freestanding Cu films are obtained by removing the Si_3N_4 and TaN using reactive ion etching (RIE) and by dissolving the protective BCB layer in an organic solvent. The advantage of the sample preparation process is that there are no restrictions on the type of film or the way the film is deposited on the substrate, as long as the Si_3N_4 etch is selective with respect to the film of interest. An alternate technique would consist of first preparing freestanding Si_3N_4 membranes, after which the film of interest can be deposited directly onto the Si_3N_4 membrane. By removing the Si_3N_4 using reactive ion etching (RIE), a freestanding film is obtained. This process is easier but much less generally applicable; the Si_3N_4 membranes are fragile, and there may be limitations with respect to which deposition techniques can be used. Moreover, for high-energy

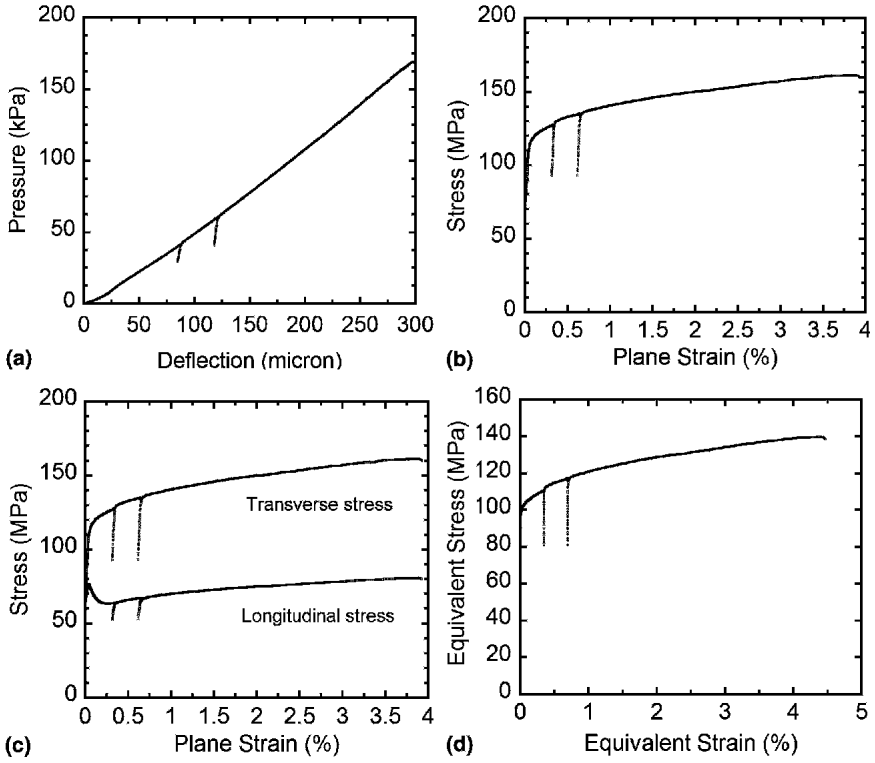

FIG. 7. Experimental results for a 2.8 μm electroplated Cu film: (a) pressure-deflection curve with two brief unloading cycles; (b) plane-strain strain-stress curve; (c) evolution of the transverse and longitudinal stress with applied strain; and (d) von Mises equivalent uniaxial stress-strain curve.

deposition techniques such as sputtering, the structure of the film deposited on the Si_3N_4 membrane may be different from that on the bulk Si substrate. The Si_3N_4 membrane does not conduct the heat of condensation away as efficiently as the Si substrate during the film deposition process, and the film over the membrane may be exposed to much higher temperatures than elsewhere. The two methods are complimentary to each other and can be applied to a wide range of materials.

Note that residual tension must be maintained in the freestanding film, since any in-plane compressive stress will cause the film to buckle due to its small bending stiffness.[24,25] Buckles near the edge of the membrane disappear only gradually as pressure is applied during an experiment, rendering the pressure-deflection data meaningless. If the stress in the film of interest is compressive, the LPCVD Si_3N_4 coating beneath the film can be kept and the composite membrane tested. The Si_3N_4 coating typically has a high tensile residual stress and the overall stress in the composite membrane may be kept in tension if the thickness ratio of the two layers is properly selected. The mechanical properties of the film of interest can be measured by subtracting the elastic contribution of the Si_3N_4 film, which can be readily determined independently.[28] This composite technique makes it possible not only to measure films with residual compression, but also to deform metal films alternating in tension and in compression. In this case, the Si_3N_4 film acts as a spring that drives the metal film into compression after unloading. This technique has been applied to Cu and Al films to study the Bauschinger effect in thin metal films.[30]

IV. EXPERIMENTAL SETUP

A schematic of the bulge test aparatus used in this study is shown in Fig. 6. The sample is clamped onto a sample holder. Pressure is applied by pumping water into the cavity under the film using a syringe pump driven by a stepper motor. The deflection at the center of the membrane is measured by means of a laser interferometer with a displacement resolution of 316.5 nm, i.e., half the wavelength of the He–Ne laser. At the beginning of each experiment, the interferometer is used to ensure that the membrane is flat and level with the surrounding substrate. The pressure is measured using a pressure gauge with a resolution of 0.1 kPa. The experiment is controlled by a computer via a LabView based program and a data-acquisition system.

V. RESULTS AND DISCUSSION

Typical pressure–deflection data for the 2.8 μm freestanding Cu film are presented in Fig. 7(a). The Cu film was loaded to a maximum deflection of approximately 300 μm, at which point it ruptured. The loading segment was interrupted by two brief unloading cycles to evaluate the elastic properties of the film. Because of the large deflection compared to the membrane width, the large deformation Eq. (6) is used to calculate the plane-strain stress–strain relationship presented in Fig. 7(b). The fracture strain is approximately 4%. From the stress–strain curve, the residual stress in the film is determined to be 66 MPa. The yield stress is defined at a specific offset plastic strain; for example, the yield stress at 0.2% plastic strain is found to be 125 MPa. The plane strain modulus $M = E/(1 - \nu^i)$ is determined from the slopes of the unloading curves and is 130 ± 5 GPa, in good agreement with the value one would expect based on the crystallographic texture of the film.[29] The plane-strain stress–strain curve [Fig. 7(b)] obtained using Eq. (6) is converted into an equivalent uniaxial stress-strain relationship [Fig. 7(d)], using the method described in the Appendix. The evolution of the transverse and longitu-

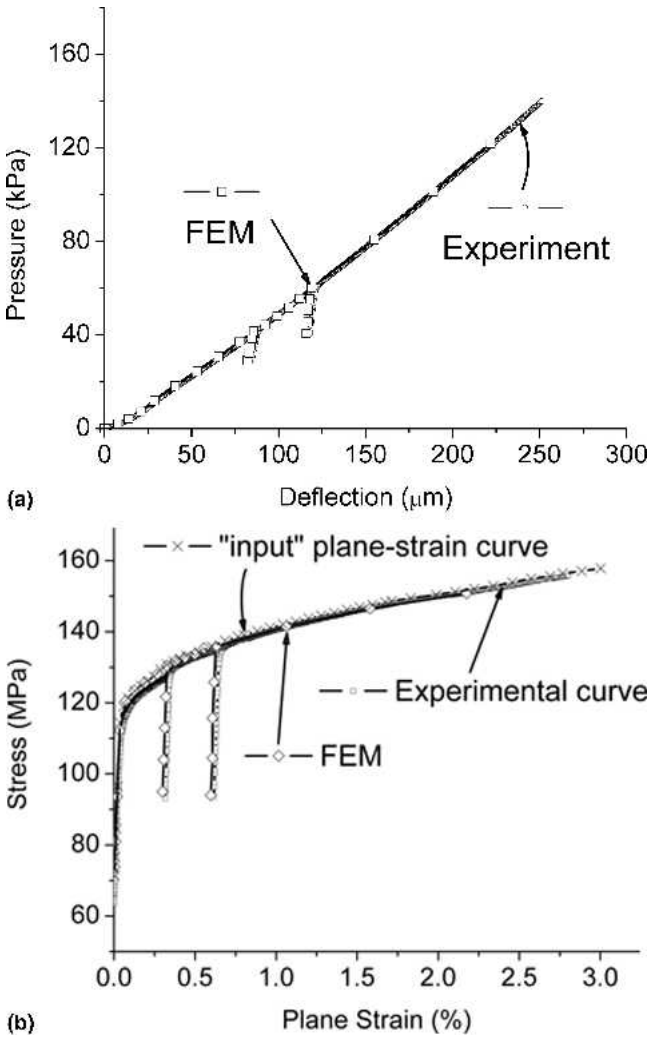

FIG. 8. Parallel FEM analysis for the experimental data: (a) the pressure-deflection curve obtained with FEM is in good agreement with the experimental curve; (b) the corresponding plane-strain stress-strain curves are compared with the "input" plane-strain behavior.

dinal stress with applied strain is presented in Fig. 7(c). The longitudinal stress first increases with applied strain and then decreases when the film starts yielding. At larger strains, the longitudinal stress increases with applied strain and is equal to half of the transverse stress, as expected for plane-strain plastic deformation. The dip in the longitudinal stress evolution curve arises because of the relatively high biaxial residual stress in the membrane: at first, the longitudinal stress is greater than half the transverse stress and decrease until its value is half the transverse stress. At this point, it starts to increase along with the transverse stress due to work hardening. When the residual stress is below a critical level, no such dip is observed. The equivalent uniaxial stress–strain curve is plotted in Fig. 7(d). The strain-hardening exponent obtained for this curve is 0.36, which is close to the value for bulk Cu.[31]

The above analysis was verified using FEM. The film thickness and membrane geometry were taken identical to the tested sample. Experimental values for elastic ($M = 130$ GPa) and plastic [Fig. 7(d)] properties were used as input for the material behavior in the FEM simulation. Poisson's ratio was taken to be 0.33. The pressure–deflection curve obtained from FEM is found to be in good agreement with the experimental data [Fig. 8(a)]. The load–deflection data obtained from FEM are then converted to a plane-strain stress–strain curve using Eq. (7). Figure 8(b) compares this stress–strain curve with the experimental curve. The agreement between numerical and experimental results is excellent and validates the experimental data analysis.

VI. CONCLUSIONS

We used FEM to analyze the plane-strain bulge test as a technique for measuring the mechanical properties of thin films, with a particular emphasis on the effects of sample aspect ratio, strain-hardening exponent, and residual stress. It was found that the analytical stress and strain formulae used to analyze the bulge test are highly accurate and that the plane-strain condition is well satisfied for all materials with strain-hardening exponents ranging from 0 to 0.5, as long as the membrane aspect ratio is 4 or greater. The residual stress mainly affects the elastic deflection of the membrane and changes the initial point of yield in the plane-strain stress–strain curve, but there is little or no effect on the rest of the stress–strain curve. The effect of the residual stress can be completely eliminated by converting the plane-strain curve into its equivalent uniaxial relationship (the von Mises stress–strain curve). The technique was applied to an electroplated Cu film. Si micromachining techniques were used to fabricate freestanding Cu membranes. Experimental results for the Cu film are in good agreement with the numerical analysis.

ACKNOWLEDGMENTS

The authors are grateful for the support from the Division of Engineering and Applied Sciences and the Materials Research Science and Engineering Center at Harvard University, Cambridge, MA. This research was funded by National Science Foundation (NSF) Grant Nos. DMR-0133559 and DMR-0215902 at Harvard University and by NSF Grant No. CMS-0407743 at Columbia University, New York, NY.

REFERENCES

1. W.D. Nix: Mechanical properties of thin-films. *Metall. Trans. A* **20,** 2217 (1989).
2. S.M. Spearing: Materials issues in microelectromechanical systems (MEMS). *Acta Mater.* **48,** 179 (2000).
3. R.P. Vinci and J.J. Vlassak: Mechanical behavior of thin films. *Ann. Rev. Mater. Sci.* **26,** 431 (1996).
4. E. Arzt: Size effects in materials due to microstructural and dimensional constraints: A comparative review. *Acta Mater.* **46,** 5611 (1998).
5. R. Venkatraman and J.C. Bravman: Separation of film thickness and grain-boundary strengthening effects in Al thin-films on Si. *J. Mater. Res.* **7,** 2040 (1992).
6. L.B. Freund and S. Suresh: *Thin Film Materials: Stress, Defect Formation, and Surface Evolution* (Cambridge University Press, New York, 2003), p. 6
7. W.C. Oliver and G.M. Pharr: Measurement of hardness and elastic modulus by instrumented indentation: Advances in understanding and refinements to methodology. *J. Mater. Res.* **19,** 3 (2004).
8. X. Chen and J.J. Vlassak: Numerical study on the measurement of thin film mechanical properties by means of nanoindentation. *J. Mater. Res.* **16,** 2974 (2001).
9. T.Y. Tsui, J.J. Vlassak, and W.D. Nix: Indentation plastic displacement field: Part I. The case of soft films on hard substrates. *J. Mater. Res.* **14,** 2196 (1999).
10. S.P. Baker, R.M. Keller-Flaig, and J.B. Shu: Bauschinger effect and anomalous thermomechanical deformation induced by oxygen in passivated thin Cu films on substrates. *Acta Mater.* **51,** 3019 (2003).
11. M.A. Haque and M.T.A. Saif: Deformation mechanisms in free-standing nanoscale thin films: A quantitative in situ transmission electron microscope study. *Proc. Natl. Acad. Sci. USA.* **101,** 6335 (2004).
12. H.B. Huang and F. Spaepen: Tensile testing of free-standing Cu, Ag and Al thin films and Ag/Cu multilayers. *Acta Mater.* **48,** 3261 (2000).
13. D.T. Read, Y.W. Cheng, R.R. Keller, and J.D. McColskey: Tensile properties of free-standing aluminum thin films. *Scripta Mater.* **45,** 583 (2001).
14. H.D. Espinosa, B.C. Prorok, and B. Peng: Plasticity size effects in free-standing submicron polycrystalline FCC films subjected to pure tension. *J. Mech. Phys. Solids* **52,** 667 (2004).
15. J.J. Vlassak and W.D. Nix: A new bulge test technique for the determination of Young's modulus and Poisson's ratio of thin films. *J. Mater. Res.* **7,** 3242 (1992).
16. J.W. Beams: Mechanical properties of thin films of gold and silver, in *Structure and Properties of Thin Films*, edited by C.A. Neugebauer, J.B. Newkirk, and D.A. Vermilyea (John Wiley and Sons, New York, 1959), p. 183.
17. O. Tabata, K. Kawahata, S. Sugiyama, and I. Igarashi: Mechanical

property measurements of thin-films using load deflection of composite rectangular membranes. *Sens. Actuators* **20,** 135 (1989).
18. H. Hencky: About the stress state in circular plates with negligible bending stiffness. *Z. Math. Phys.* **63,** 311 (1915), in German.
19. J.J. Vlassak: New experimental techniques and analysis methods for the study of mechanical properties of materials in small volumes. Ph.D. Dissertation, Stanford University, Stanford, CA, 1994.
20. S. Levy: Large deflection theory for rectangular plates, in *Nonlinear Problems in Mechanics of Continua*, edited by E. Reissner, W. Prager, and J.J. Stoker (Proc. Symposia. Appl. Math. **I**, Am. Math. Soc., New York, 1949), p. 197.
21. P. Lin: The in-situ measurement of mechanical properties of multi-layer coatings. Ph.D. Dissertation, Massachusetts Institute of Technology, Cambridge, MA, 1990.
22. S. Timoshenko and S. Woinowsky-Krieger: *Theory of Plates and Shells* (McGraw-Hill, New York, 1959), p. 580
23. H. Itozaki: Mechanical properties of composition modulated copper-palladium foils. Ph.D. Dissertation, Northwestern University, Evanston, IL, 1982.
24. M.K. Small and W.D. Nix: Analysis of the accuracy of the bulge test in determining the mechanical properties of thin-films. *J. Mater. Res.* **7,** 1553 (1992).
25. M.K. Small, J.J. Vlassak, and W.D. Nix: Re-examining the bulge test: Methods for improving accuracy and reliability, in *Thin Films: Stresses and Mechanical Properties III*, edited by W.D. Nix, J.C. Bravman, E. Arzt, and L.B. Freund (Mater. Res. Soc. Symp. Proc. **239,** Pittsburgh, PA, 1992), p. 257.
26. Y. Xiang, X. Chen, and J.J. Vlassak: The mechanical properties of electroplated Cu thin films measured by means of the bulge test technique, in *Thin Films: Stresses and Mechanical Properties IX*, edited by C.S. Ozkan, L.B. Freund, R.C. Cammarata, and H. Gao (Mater. Res. Soc. Symp. Proc. **695,** Warrendale, PA, 2002), p. 189.
27. F. Maseeh and S.D. Senturia: Viscoelasticity and creep recovery of polyimide thin films, in *Technical Digest. IEEE Solid-State Sensor and Actuator Workshop*, edited by IEEE (IEEE, NY, 1990), p. 55.
28. Y. Xiang, T.Y. Tsui, J.J. Vlassak, and A.J. McKerrow: Measuring the elastic modulus and ultimate strength of low-k dielectric materials by means of the bulge test, in *the Proceedings of IEEE 2004 International Interconnect Technology Conference*, edited by IEEE (IEEE, Piscataway, NJ, 2004), p. 133.
29. M.T. Perez-Prado and J.J. Vlassak: Microstructural evolution in electroplated Cu thin films. *Scripta Mater.* **47,** 817 (2002).
30. Y. Xiang and J.J. Vlassak: Bauschinger effect in thin metal films. *Scripta Mater.* **53,** 177 (2005).
31. G.E. Dieter: *Mechanical Metallurgy,* 3rd ed. (McGraw-Hill, New York, 1986), p. 287.
32. L.B. Freund, personal communication (1995).
33. M. Azrin and W.A. Backofen: The deformation and failure of a biaxially stretched sheet. *Metall. Trans.* **1,** 2857 (1970).

APPENDIX

The stress–strain curves obtained in the bulge test are plane-strain stress–strain curves. These curves can be converted into equivalent uniaxial stress–strain curves using an analysis first suggested by Freund.[32] This analysis eliminates the effect of the residual stress on the stress–strain curves and facilitates comparison of experimental bulge test data with results obtained from uniaxial tension tests.

The three principal stress directions of the freestanding film are shown in Fig. 1(A). Since the pressure applied to the film is much smaller compared to the in-plane stress, σ_3 can be taken equal to zero during the experiment. Initially, when the applied pressure is zero, the film has an equi-biaxial residual stress $\sigma_1 = \sigma_2 = \sigma_0$. During the experiment, σ_1 are ϵ_1 are measured. In the elastic regime σ_2 can be determined through Poisson's effect:

$$\sigma_2 = \sigma_0 + \nu(\sigma_1 - \sigma_0) \quad , \tag{A1}$$

as a result of the plane-strain condition.

In the following analysis, the material is assumed to obey the J_2 flow theory. Considering $\sigma_3 = 0$, the von Mises equivalent stress $\bar{\sigma}$ is given by

$$\bar{\sigma} = (\sigma_1^2 - \sigma_1\sigma_2 + \sigma_2^2)^{1/2} \quad , \tag{A2}$$

where σ_1 is measured, σ_2 is given by Eq. (A1) in the elastic regime and is yet to be determined in the plastic regime. The equivalent plastic strain $\bar{\epsilon}_p$ is a function of the equivalent stress $\bar{\sigma}$

$$\bar{\epsilon}_p = g(\bar{\sigma}) \quad . \tag{A3}$$

The flow rates associated with the von Mises criterion are in this case:

$$\dot{\epsilon}_1^p = \frac{\sigma_1 - 1/2\sigma_2}{\bar{\sigma}}\, g'(\bar{\sigma})\dot{\bar{\sigma}} \quad ,$$

$$\dot{\epsilon}_2^p = \frac{\sigma_2 - 1/2\sigma_1}{\bar{\sigma}}\, g'(\bar{\sigma})\dot{\bar{\sigma}} \quad , \tag{A4}$$

where $g'(\bar{\sigma}) = (d\bar{\epsilon}_p/d\bar{\sigma})$. In the experimental configuration here, the response is rate-independent, and σ_1 increases monotonically with time. As a result, time can be replaced with σ_1 in the above equations. By writing out the equation for the strain rates in the longitudinal and transverse directions along with the plane-strain constraints, we find

$$\begin{cases} \dfrac{d\epsilon_1}{d\sigma_1} = \dfrac{1}{E}\left(1 - \nu\dfrac{d\sigma_2}{d\sigma_1}\right) + \dfrac{\sigma_1 - \frac{1}{2}\sigma_2}{\bar{\sigma}}\dfrac{dg}{d\sigma_1} \quad , \\ \dfrac{d\epsilon_2^e}{d\sigma_1} = \dfrac{1}{E}\left(\dfrac{d\sigma_2}{d\sigma_1} - \nu\right) \quad , \\ \dfrac{d\epsilon_2^p}{d\sigma_1} = \dfrac{\sigma_2 - \frac{1}{2}\sigma_1}{\bar{\sigma}}\dfrac{dg}{d\sigma_1} \quad , \\ \dfrac{d\epsilon_2^e}{d\sigma_1} + \dfrac{d\epsilon_2^p}{d\sigma_1} = 0 \quad . \end{cases} \tag{A5}$$

These equations are solved for $(dg/d\sigma_1)$ and $(d\sigma_2/d\sigma_1)$, resulting in the following differential equations

$$\begin{cases} \dfrac{d\sigma_2}{d\sigma_1} = \nu - \dfrac{E\left(\dfrac{1-\nu^2}{E} - \dfrac{d\epsilon_1}{d\sigma_1}\right)(\sigma_1 - 2\sigma_2)}{\sigma_1(2-\nu) - \sigma_2(1-2\nu)} \quad , \\ \dfrac{dg}{d\sigma_1} = \dfrac{2\bar{\sigma}\left(\dfrac{d\epsilon_1}{d\sigma_1} - \dfrac{1-\nu^2}{E}\right)}{\sigma_1(2-\nu) - \sigma_2(1-2\nu)} \quad . \end{cases} \tag{A6}$$

Noting that the plane-strain modulus is $M = E/(1 - \nu^2)$ and the tangential plane-strain modulus is $M_t = (d\sigma_1/d\epsilon_1)$, the above equations are revised to

$$\begin{cases} \dfrac{d\sigma_2}{d\sigma_1} = \nu - \dfrac{E\left(\dfrac{1}{M} - \dfrac{1}{M_t}\right)(\sigma_1 - 2\sigma_2)}{\sigma_1(2 - \nu) - \sigma_2(1 - 2\nu)} \\ \dfrac{dg}{d\sigma_1} = \dfrac{2\bar{\sigma}\left(\dfrac{1}{M_t} - \dfrac{1}{M}\right)}{\sigma_1(2 - \nu) - \sigma_2(1 - 2\nu)} \end{cases}, \quad . \tag{A7}$$

By integrating equations (A7), the longitudinal stress σ_2 and the equivalent stress–strain curve $\bar{\epsilon}_p$ can be derived from an experimental measurement of $\sigma_1(\epsilon_1)$. In practice, the plane-strain modulus M is determined from the unloading sections of the measured $\sigma_1(\epsilon_1)$ curve, and the tangential plane-strain modulus M_t at each point can be obtained by a linear fit to adjacent data points. Poisson's ration ν can be taken as equal to the bulk value or needs to be determined from an independent measurement. The initial value of σ_2 is obtained from Eq. (A1) in the elastic regime. With these parameters, the above differential equations can be numerically solved to get the equivalent strain $\bar{\epsilon}_p$ and the longitudinal stress σ_2, thus obtaining the von Mises equivalent stress $\bar{\sigma}$ using equation (A2). The resulting $\bar{\sigma}$–$\bar{\epsilon}_p$ curve is the equivalent uniaxial stress–strain curve. This numerical solution can be readily implemented in a spreadsheet.